Phase behavior of confined symmetric binary mixtures

Dirk Woywod* and Martin Schoen†

Stranski-Laboratorium für Physikalische und Theoretische Chemie, Sekretariat TC 7, Fakultät für Mathematik und Naturwissenschaften, Technische Universität Berlin, Straße des 17. Juni 124, D-10623 Berlin, Germany

(Received 10 September 2002; published 26 February 2003)

We employ mean-field lattice density functional theory to investigate the phase behavior of a binary (A-B) mixture confined to nanoscopic slit pores with chemically homogeneous walls. We consider only nearest-neighbor interactions in symmetric mixtures, where $\epsilon_{AA}=\epsilon_{BB}\neq\epsilon_{AB}$ and ϵ is a measure of attraction between molecules of like (subscripts AA and BB) and unlike species (subscript AB), respectively. In addition, molecules are exposed to short-range attraction by the substrates separated by z lattice planes where ϵ_W is the relevant coupling parameter. Moreover, the chemical potentials of both components are the same, that is, $\mu_A=\mu_B=\mu$. In thermodynamic equilibrium (for fixed temperature T and chemical potential μ) the grand-potential density $\omega[\boldsymbol{\rho},\boldsymbol{m}]$ ($\boldsymbol{\rho}\equiv\{\rho_1,\ldots,\rho_z\}$, $\boldsymbol{m}\equiv\{m_1,\ldots,m_z\}$) assumes a global minimum which we find by minimizing ω numerically with respect to the order parameters $\rho_l\equiv\rho_l^A+\rho_l^B$ (total local density) and $m_l\equiv(\rho_l^A-\rho_l^B)/\rho_l$ (local "miscibility") at lattice plane l parallel to the pore walls. By varying ϵ_{AB} three generic types of bulk phase diagrams are observed. On account of confinement (i.e., by varying ϵ_W as well as z) one may switch between these different types of phase diagrams. This may have profound practical repercussions for experimental nanophase separation since depending on pore width and chemical nature of its walls a bulk gas mixture may undergo capillary condensation and form either a stable mixed or demixed liquid phase.

DOI: 10.1103/PhysRevE.67.026122 PACS number(s): 05.70.Np, 61.46.+w, 68.55.Nq, 68.55.−a

I. INTRODUCTION

The phase behavior of pure fluids and their mixtures in confined geometries is currently receiving a lot of experimental and theoretical attention (for a recent review see Ref. [1]). Experimentally one is usually concerned with confining solid matrices of either low porosity like porous glasses [2–8] or high porosity like silica gels [9–12]. These systems are studied by a variety of techniques including light or neutron scattering [5,6,9–11], measurements of nonlinear dielectric phenomena [4], and of the heat capacity [2]. Typical pore widths range from 1 to 100 nm.

Theoretically, a variety of model binary mixtures has been investigated within the framework of different techniques. Most of these works are concerned with so-called symmetric mixtures characterized by identical interactions between like molecules of both species. Several theoretical studies focus on domain growth during phase separation in confined geometry [13–20] which is described by a power law in three-dimensional systems [19]. By means of computer simulations associating fluid mixtures are investigated with particular emphasis on the formation of hydrogen bonds [17]. Within the framework of Monte Carlo simulations in the grand canonical ensemble (GCEMC), Gózdz *et al.* determined aspects of the phase diagram of a binary mixture in slit pores that are in thermodynamic equilibrium with a demixed bulk mixture [21]. Also by means of GCEMC, Cushman and Curry studied binary mixtures of "simple" fluids confined between nanoscopically corrugated substrate surfaces [22,23]. In their system the substrates are decorated with rectilinear grooves promoting (partial) solidification of the confined mixture. Grabowski *et al.* employed Monte Carlo simulations to investigate wetting of solid surfaces by binary-mixture films [24]. In GCEMC simulations by Kierlik *et al.* [25], the impact of independently varying the chemical potentials μ_A and μ_B of both components is investigated. These authors observe that mere confinement by nonselective substrates causes selective adsorption of the dilute component.

Besides computer simulations density functional calculations [25,26] and integral–equation approaches [27,28] have also been employed to investigate properties of confined binary mixtures. Pizio *et al.* [26] are concerned with the effect of polydispersity in hard-sphere mixtures, whereas Trokhymchuk *et al.* [27] focus on chemical reactions. In both cases the mixture is confined to nanoscopic slits. On the contrary, Schöll-Paschinger and co-workers consider a random porous matrix formed by immobile hard spheres of a given number density [28] which serves as a suitable model for experimental situations where the confining matrix is a porous glass. Another powerful theoretical tool are self-consistent field calculations [29] which have been used by Binder *et al.* [30] to study symmetric binary polymer blends in confinement.

Unlike these previous works, we are concerned here with a systematic study of the phase behavior of binary mixtures composed of simple fluids confined to ordered nanoporous matrices. Examples of such materials are MCM-41 or SBA-15 silicas that can relatively routinely be synthesized [31] and in which sorption isotherms can be measured relatively easily [32]. To determine the phase behavior of binary mixtures in such nanoscopic pores theoretically we extend a previous study by Bock *et al.*, who were concerned with pure fluids, to the case of symmetric binary mixtures [33]. In Ref. [33], lattice density functional theory is employed to investigate the interplay between surface-induced and confinement-induced phase transitions in slit pores with chemically patterned substrates. In addition to discretization of configuration space, Bock *et al.* treat the (intrinsic) free-

*Electronic address: dirk.woywod@fluids.tu-berlin.de

†Electronic address: martin.schoen@fluids.tu-berlin.de

energy functional at mean-field level [33] which is believed to be sufficiently realistic as far as first-order phase transitions are concerned [34].

In this work, we focus exclusively on the impact of the degree of confinement (i.e., the pore width) and the strength of the fluid-substrate attraction on the phase behavior of confined binary mixtures of species A and B, say. Like most previous workers, we restrict ourselves to symmetric mixtures characterized by an equally strong attraction between like molecules of either species. Moreover, we focus exclusively on the case $\mu_A=\mu_B$. Thus, mixture properties come about only by varying the attraction strength between unlike molecules. For such somewhat simplistic mixtures Wilding *et al.* determined the bulk phase behavior [35]. While also using a mean-field approach, Wilding *et al.* are concerned with an off-lattice model [35]. Depending on characteristic ranges of the A-B attraction strength they find three distinctly different generic types of phase diagrams (see Fig. 1 in Ref. [35]). We will show here that the same generic types of bulk phase diagrams are observed in lattice models, too. Moreover, we shall demonstrate that on account of mere confinement it is possible to switch from one type of these phase diagrams to another which may have profound consequences for liquid-liquid nanophase separation in ordered porous matrices.

The remainder of this paper is organized as follows. In Sec. II, we outline the theoretical framework where, in particular, we introduce the lattice-gas model in Sec. II A and develop its mean-field treatment in Sec. II B. The solution of our model proceeds numerically. We outline the numerical procedure in Sec. III. Its key ingredient are analytical solutions at vanishing temperature which we discuss in Sec. III A, whereas Sec. III B is devoted to the more general case of solutions for nonvanishing temperatures. Results are summarized in Sec. IV, where we begin in Sec. IV A with a brief discussion of bulk phase diagrams. Sections IV B and IV C are given, respectively, to analyses of confinement effects and confinement-controlled decomposition of binary mixtures. In Sec. V, we summarize our key findings.

II. THEORY

A. Lattice model

Consider a binary (A-B) fluid mixture confined to a slit pore whose substrate surfaces are planar and chemically homogeneous. To simplify the treatment, we discretize space such that positions of molecules are restricted to the $\mathcal{N}=nz$ sites of a simple-cubic lattice, whose lattice constant is ℓ. The position of a fluid molecule on the lattice may then be specified by a pair of integers (k,l), where $1\leqslant k\leqslant n$ labels the position in the x-y plane and $1\leqslant l\leqslant z$ determines the position of this plane relative to the substrate surfaces. Accordingly, we introduce the $n\times z$ matrix $\mathbf{s}$ of occupation numbers whose elements are given by

$$s_{k,l}=\begin{cases}+1 & \text{site occupied by molecule of component } A\\ 0 & \text{empty site}\\ -1 & \text{site occupied by molecule of component } B.\end{cases} \tag{2.1}$$

From Eq. (2.1) it is straightforward to work out expressions for the total number of sites $N_A(\mathbf{s})$ and $N_B(\mathbf{s})$ occupied by molecules of species A and B, respectively. One obtains

$$N_A(\mathbf{s})=\frac{1}{2}\sum_{k=1}^{n}\sum_{l=1}^{z}(s_{k,l}+1)s_{k,l}=\frac{1}{2}\sum_{k=1}^{n}\sum_{l=1}^{z}(s_{k,l}^2+s_{k,l}), \tag{2.2a}$$

$$N_B(\mathbf{s})=\frac{1}{2}\sum_{k=1}^{n}\sum_{l=1}^{z}(s_{k,l}-1)s_{k,l}=\frac{1}{2}\sum_{k=1}^{n}\sum_{l=1}^{z}(s_{k,l}^2-s_{k,l}), \tag{2.2b}$$

such that

$$N(\mathbf{s})=N_A(\mathbf{s})+N_B(\mathbf{s})=\sum_{k=1}^{n}\sum_{l=1}^{z}s_{k,l}^2 \tag{2.3}$$

is the total number of *occupied* sites in a given configuration $\mathbf{s}$ (i.e., for a given occupation–number pattern).

Moreover, it is straightforward to verify that the total number of molecules of species A at either substrate is given by

$$N_{AW}(\mathbf{s})=\frac{1}{2}\sum_{k=1}^{n}[(1+s_{k,1})s_{k,1}+(1+s_{k,z})s_{k,z}], \tag{2.4}$$

which follows from considerations similar to the ones leading to Eq. (2.2a). Thus, the total number of molecules of species B at the substrate is given by

$$N_{BW}(\mathbf{s})=-\frac{1}{2}\sum_{k=1}^{n}[(1-s_{k,1})s_{k,1}+(1-s_{k,z})s_{k,z}]. \tag{2.5}$$

Similarly, one can work out expressions for the number N_{AA} (N_{BB}) of A-A (B-B) pairs, that is, directly connected sites both of which are occupied by a molecule of species A (B). These somewhat more involved expressions are given by

$$N_{AA}(\mathbf{s})=\frac{1}{8}\sum_{k=1}^{n}\sum_{l=1}^{z}s_{k,l}(1+s_{k,l})\Bigg[s_{k,l+1}(1+s_{k,l+1})+s_{k,l-1}(1+s_{k,l-1})+\sum_{m=1}^{\mathrm{NN}(k)}s_{m,l}(1+s_{m,l})\Bigg], \tag{2.6a}$$

$$N_{BB}(\mathbf{s})=\frac{1}{8}\sum_{k=1}^{n}\sum_{l=1}^{z}s_{k,l}(1-s_{k,l})\Bigg[s_{k,l+1}(1-s_{k,l+1})+s_{k,l-1}(1-s_{k,l-1})+\sum_{m=1}^{\mathrm{NN}(k)}s_{m,l}(1-s_{m,l})\Bigg], \tag{2.6b}$$

where the summation over m extends over the 4 nearest neighbors $\mathrm{NN}(k)$ of lattice site k in the x-y plane. A slightly more complicated expression obtains for the number of A-B (nearest-neighbor) pairs, namely,

$$N_{AB}(\mathbf{s}) = -\frac{1}{8}\sum_{k=1}^{n}\sum_{l=1}^{z}\left\{ s_{k,l}(1+s_{k,l})\left[s_{k,l+1}(1-s_{k,l+1}) + s_{k,l-1}(1-s_{k,l-1}) + \sum_{m=1}^{\mathrm{NN}(k)} s_{m,l}(1-s_{m,l})\right]\right.$$
$$\left. + s_{k,l}(1-s_{k,l})\left[s_{k,l+1}(1+s_{k,l+1}) + s_{k,l-1} \times (1+s_{k,l-1}) + \sum_{m=1}^{\mathrm{NN}(k)} s_{m,l}(1+s_{m,l})\right]\right\}. \quad (2.7)$$

Because of the infinite repulsion ''felt'' by fluid molecules at vanishing distance from the substrate surface, we amend Eqs. (2.6) and (2.7) by the boundary conditions

$$s_{k,0} = s_{k,z+1} = 0 \quad \forall k. \quad (2.8)$$

Based upon these expressions, we can cast the ''Hamiltonian'' of our binary lattice-gas mixture as

$$H(\mathbf{s}) = \epsilon[N_{AA}(\mathbf{s}) + N_{BB}(\mathbf{s})] + \epsilon_{AB}N_{AB}(\mathbf{s}) + \epsilon_W[N_{AW}(\mathbf{s}) + N_{BW}(\mathbf{s})] - \mu[N_A(\mathbf{s}) + N_B(\mathbf{s})]. \quad (2.9)$$

In Eq. (2.9), $\epsilon = \epsilon_{AA} = \epsilon_{BB} \leqslant 0$ is the depth of the attractive well of a square-well potential governing the interaction between like fluid molecules (symmetric mixture). Similarly, $\epsilon_{AB} \leqslant 0$ determines the attraction strength between unlike fluid molecules. Since the width of the attractive well is taken to be equal to the lattice constant ℓ in both cases, we effectively restrict our model to nearest-neighbor interactions only. Likewise, we assume for both species the same square-well fluid-substrate potential (i.e., nonselective walls) where the range of the attraction is again equal to ℓ and the interaction strength is represented by $\epsilon_W \leqslant 0$. Since we allow each site to be occupied by one molecule (of species A or B) at most, we implicitly account for the hard-core repulsion between pairs of fluid molecules and between each fluid molecule and the substrate. In Eq. (2.9), μ denotes the (partial) chemical potential which we again consider to be the same for both species A and B.

B. Thermodynamics and mean-field approximation

To simplify the subsequent treatment, we replace the Hamiltonian in Eq. (2.9) by its mean-field analog

$$H_{\mathrm{MF}}(\boldsymbol{\rho},\mathbf{m}) = n\left\{ \frac{\epsilon}{4}\sum_{l=1}^{z} \rho_l[\rho_{l+1}(1+m_l m_{l+1}) + \rho_{l-1}(1+m_l m_{l-1}) + 4\rho_l(1+m_l^2)] + \frac{\epsilon_{AB}}{4}\sum_{l=1}^{z} \rho_l[\rho_{l+1}(1-m_l m_{l+1}) + \rho_{l-1}(1-m_l m_{l-1}) + 4\rho_l(1-m_l^2)] + \epsilon_W(\rho_1+\rho_z) - \sum_{l=1}^{z}\rho_l\mu\right\}. \quad (2.10)$$

In Eq. (2.10), $\boldsymbol{\rho} \equiv \{\rho_1, \ldots, \rho_z\}$ and $\mathbf{m} \equiv \{m_1, \ldots, m_z\}$ are sets of local order parameters, where

$$\rho_l \equiv \rho_l^A + \rho_l^B = \frac{1}{n}\sum_{m=1}^{n} s_{m,l}^2 \quad (2.11)$$

is the *total* mean (local) density across the x-y plane located at l. In Eq. (2.11) ρ_l^A and ρ_l^B are the associated *partial* mean (local) densities of components A and B, respectively. They are defined in units of ℓ^3 such that $0 \leqslant \rho_l \leqslant 1$. The ''miscibility'' parameter m_l defined through

$$m_l\rho_l \equiv \rho_l^A - \rho_l^B = \frac{1}{n}\sum_{i=1}^{n} s_{i,l} \quad (2.12)$$

is a quantitative measure of the degree of local decomposition of the binary mixture such that $-1 \leqslant m_l \leqslant 1$. For example, if at plane l the fluid consists of pure component A, $\rho_l^B = 0$, so that $\rho_l = \rho_l^A$. Equation (2.12), thus, implies $m_l = 1$. Likewise, if at plane l pure component B is present, $\rho_l = \rho_l^B$ and hence $m_l = -1$. If, on the other hand, we have perfect miscibility across plane l, $\rho_l^A = \rho_l^B$ [subject to Eq. (2.11) and the constraint $\rho_l \leqslant 1$] and hence $m_l = 0$. In other words, the phase behavior of the binary mixture is characterized by two sets of *local* order parameters, namely, $\boldsymbol{\rho} \equiv \{\rho_1, \ldots, \rho_z\}$ and $\mathbf{m} \equiv \{m_1, \ldots, m_z\}$.

From a microscopic perspective the number of *a priori* possible configurations at fixed $\mathcal{N}$, ρ_l, and m_l is given by the combinatorial expression

$$\Omega(\boldsymbol{n},\mathbf{m}) = \prod_{l=1}^{z}\binom{n}{n_l}\binom{n_l}{n_l^A} = \prod_{l=1}^{z}\frac{n!}{(n-n_l)!\left(n_l\frac{1+m_l}{2}\right)!\left(n_l-n_l\frac{1+m_l}{2}\right)!} = \prod_{l=1}^{z}\frac{n!}{(n-n_l)!\left(n_l\frac{1+m_l}{2}\right)!\left(n_l\frac{1-m_l}{2}\right)!}, \quad (2.13)$$

where elements of the z-dimensional vector $\boldsymbol{n} \equiv \{n_1, \ldots, n_z\}$ correspond to the number of sites occupied by molecules of either species in lattice plane l and, therefore, $n_l = n\rho_l$. The number of molecules of species A and B across lattice plane l is given by $n_l^A = n_l(1+m_l)/2$, and $n_l^B = n_l - n_l^A = n_l(1-m_l)/2$, respectively.

Since we are concerned with the thermodynamic limit both integers $n, n_l \to \infty$, so that both ρ_l and m_l are continuous on the interval $[0,1]$ and $[-1,1]$, respectively. Hence, using Stirling's approximation, we may rewrite Eq. (2.13) as

$$\lim_{n,\{n_l\}\to\infty}\Omega(\boldsymbol{n},\boldsymbol{m})=\prod_{l=1}^{z}\frac{n^n}{(n-n_l)^{n-n_l}\left(n_l\frac{1+m_l}{2}\right)^{n_l(1+m_l)/2}\left(n_l\frac{1-m_l}{2}\right)^{n_l(1-m_l)/2}}. \tag{2.14}$$

Introducing the grand canonical ensemble partition function Ξ in mean-field approximation

$$\Xi=\Omega\exp(-\beta H_{\mathrm{MF}}), \tag{2.15}$$

we define the grand-potential density

$$\omega\equiv-\frac{1}{\beta\mathcal{N}}\ln\Xi=-\frac{1}{\beta\mathcal{N}}\ln\Omega+\frac{H_{\mathrm{MF}}}{\mathcal{N}}=\omega(T,\mu)|_{\rho_l,m_l}, \tag{2.16}$$

where $\beta=1/k_BT$ (k_B Boltzmann's constant, T temperature).

At fixed T, we may, thus, write

$$\frac{d\omega}{d\mu}=\sum_{l=1}^{z}\left(\frac{\partial\omega}{\partial\rho_l}\frac{d\rho_l}{d\mu}+\frac{\partial\omega}{\partial m_l}\frac{dm_l}{d\mu}\right)+\frac{\partial\omega}{\partial\mu}. \tag{2.17}$$

At thermodynamic equilibrium ω assumes a global minimum with respect to variations of the (sets of local) order parameters $\boldsymbol{\rho}$ and $\boldsymbol{m}$. The necessary condition for its existence may be stated as ($T=$const)

$$\frac{\partial\omega}{\partial\rho_l}=0, \tag{2.18a}$$

$$\frac{\partial\omega}{\partial m_l}=0\quad\forall l. \tag{2.18b}$$

From Eq. (2.17) this implies

$$\frac{d\omega}{d\mu}=\frac{\partial\omega}{\partial\mu}=-\overline{\rho}, \tag{2.19}$$

where the far right side follows from Eq. (A1) and $\overline{\rho}\equiv z^{-1}\Sigma_{l=1}^{z}\rho_l$ is the total mean density of the lattice gas. As shown in the Appendix, Eqs. (2.18) lead to $2z$ coupled transcendental equations which may be cast compactly as

$$g_1(\rho_l,m_l)=\rho_{l+1}+\rho_{l-1}, \tag{2.20a}$$

$$g_2(\rho_l,m_l)=\rho_{l+1}m_{l+1}+\rho_{l-1}m_{l-1},\quad l=1,\ldots,z, \tag{2.20b}$$

together with the boundary conditions $\rho_0=\rho_{z+1}=0$ [see Eq. (2.8)] imposed by the infinitely repulsive core of the substrates. The functions g_1 and g_2 are defined in Eqs. (A5) and (A4), respectively.

III. NUMERICAL PROCEDURE

To solve Eqs. (2.20), we resort to a numerical procedure detailed below in Sec. III B. It requires suitable starting solutions which we obtain by first considering the limit $T=0$. Since in this limit entropic contributions vanish, the grand-potential density is given by the expression displayed in Eq. (A6) which has to be evaluated for all possible phases (i.e., morphologies) $\mathcal{P}$ of the confined binary mixture which we shall identify promptly in Sec. III A.

A. The limit of vanishing temperature

To identify phases of confined binary mixtures at $T=0$, we begin by realizing that in our model two energetically distinct groups of lattice sites can be distinguished: ''wall'' sites (subscript w) $l=1,z$, where molecules of both species are surrounded by five nearest neighbors and are subject to the interaction with the substrate; ''inner'' sites (subscript i) $2\leqslant l\leqslant z-1$, where each molecule is surrounded by six nearest neighbors but does not interact with either substrate. For $T=0$, ρ_{i}, and ρ_{w} are discrete and can independently assume the values 0 (empty x-y plane) and 1 (completely occupied x-y plane). If the latter is true the plane in question can be occupied either by molecules of species A ($m_{\mathrm{i,w}}=1$), B ($m_{\mathrm{i,w}}=-1$), or by an equimolar mixture of both components ($m_{\mathrm{i,w}}=0$).

Following the modular approach introduced by Bock *et al.* [33], the local order parameters ρ_l and m_l at $T=0$ have to have the same value for all sites l pertaining to the same energetically distinct group of lattice sites. Thus, from a conceptual perspective it will prove sensible to define a phase $\mathcal{P}$ as the set

$$\mathcal{P}\equiv\{\rho_{\mathrm{w}},m_{\mathrm{w}}\rho_{\mathrm{w}},\rho_{\mathrm{i}},m_{\mathrm{i}}\rho_{\mathrm{i}}\}. \tag{3.1}$$

From the above considerations it then follows that 16 different phases are *in principle* conceivable at most in the limit $T=0$. They are summarized in Table I.

Since we are dealing with the special case of a symmetric binary mixture, several phases (labeled by an asterisk in Table I) may be neglected beforehand because they are energetically and structurally equivalent to one of the remaining entries in that Table. For example, entries two and four are equivalent since it does not matter whether ''inner'' sites are occupied by molecules of species A or B because the two are themselves indistinguishable. Similar logic prompts us to conclude that only ten out of the original 16 phases need to be considered explicitly, henceforth.

In principle, each phase $\mathcal{P}^\alpha$ may coexist with another one $\mathcal{P}^\beta$, say. Thus, 45 such pairs need to be considered explicitly. Mathematically speaking, $\mathcal{P}^\alpha$ and $\mathcal{P}^\beta$ coexist at a chemical potential $\mu^{\alpha\beta}$ defined through the equation

$$\omega^\alpha(\mu^{\alpha\beta})=\omega^\beta(\mu^{\alpha\beta}),\quad T=0, \tag{3.2}$$

where ω^α and ω^β are obtained from Eq. (A6). If ω^α is the global minimum of the grand-potential density, $\mu_{\mathrm{x}}^{\alpha\beta}\equiv\mu^{\alpha\beta}$

TABLE I. Lattice-gas phases $\mathcal{P}$ at $T=0$ [see Eq. (3.1)]. The subscripts w and i refer to sites $z=1,z$ and $2\leqslant z\leqslant z-1$, respectively. For symmetric binary mixtures phases labeled by an asterisk are obsolete (see text).

$\mathcal{P}$	ρ_w	$m_w\rho_w$	ρ_i	$m_i\rho_i$
1	0	0	0	0
2*	0	0	1	−1
3	0	0	1	0
4	0	0	1	1
5*	1	−1	0	0
6*	1	−1	1	−1
7*	1	−1	1	0
8*	1	−1	1	1
9	1	0	0	0
10	1	0	1	−1
11	1	0	1	0
12	1	0	1	1
13	1	1	0	0
14*	1	1	1	−1
15	1	1	1	0
16	1	1	1	1

is the chemical potential at which $\mathcal{P}^\alpha$ and $\mathcal{P}^\beta$ are coexisting phases in thermodynamic equilibrium with each other.

B. Nonvanishing temperatures

For $T>0$, we need to determine the sets of order local parameters $\boldsymbol{\rho}$ and $\boldsymbol{m}$ by solving Eqs. (2.20) simultaneously. However, for nonvanishing temperatures both local densities and mixing parameters are no longer discrete as before at $T=0$ but continuous on the intervals $[0,1]$ and $[-1,1]$, respectively. A solution of Eqs. (2.20) may then be achieved numerically adopting an iterative scheme detailed below.

Let us begin by reintroducing the set of (local) order parameters via the $2z$-dimensional vector

$$\boldsymbol{x}=\begin{pmatrix}\rho_1\\ m_1\\ .\\ .\\ .\\ \rho_z\\ m_z\end{pmatrix}. \tag{3.3}$$

Equations (2.20) can then be rewritten in vector notation as

$$\boldsymbol{f}(\boldsymbol{x})=\begin{pmatrix} g_1(\rho_1,m_1)-\rho_2-\rho_0\\ g_2(\rho_1,m_1)-\rho_2 m_2-\rho_0 m_0\\ .\\ .\\ .\\ g_1(\rho_z,m_z)-\rho_{z+1}-\rho_{z-1}\\ g_2(\rho_z,m_z)-\rho_{z+1}m_{z+1}-\rho_{z-1}m_{z-1}\end{pmatrix}=\boldsymbol{0}. \tag{3.4}$$

Suppose a solution $\boldsymbol{x}_0$ of Eq. (3.4) is already known for some T_0 and μ_0. We are then seeking a solution $\boldsymbol{x}$ of Eq. (3.4) for a given

$$T=T_0+\delta T, \tag{3.5a}$$

$$\mu=\mu_0+\delta\mu. \tag{3.5b}$$

This new solution is obtained iteratively. Provided δT and $\delta\mu$ are sufficiently small, a suitable iteration scheme can be obtained by first expanding $\boldsymbol{f}(\boldsymbol{x})$ in a Taylor series around some $\boldsymbol{x}_i$ truncated after the linear term, that is,

$$\boldsymbol{f}(\boldsymbol{x})=\boldsymbol{f}(\boldsymbol{x}_i)+\boldsymbol{\nabla}\cdot\boldsymbol{f}^T(\boldsymbol{x})\big|_{x=x_i}\cdot(\boldsymbol{x}-\boldsymbol{x}_i)+O(|\boldsymbol{x}-\boldsymbol{x}_i|^2)\equiv 0, \tag{3.6}$$

where the $2z$-dimensional vector $\boldsymbol{\nabla}\equiv(\partial/\partial\rho_1,\partial/\partial m_1,\ldots,\partial/\partial\rho_z,\partial/\partial m_z)^T$. Equation (3.6) can be recast as

$$\boldsymbol{x}_{i+1}=-(\boldsymbol{\nabla}\cdot\boldsymbol{f}^T(\boldsymbol{x})\big|_{x=x_i})^{-1}\cdot\boldsymbol{f}(\boldsymbol{x}_i)+\boldsymbol{x}_i. \tag{3.7}$$

Equation (3.7) is then iterated until $|\boldsymbol{f}(\boldsymbol{x}_i)|\leqslant 10^{-11}$. One can easily verify from the definition in Eq. (3.4) that the matrix $\boldsymbol{\nabla}\cdot\boldsymbol{f}^T$ has band structure and can therefore be inverted numerically quite efficiently even if z becomes large; note that in the limiting case of a bulk system $\boldsymbol{\nabla}\cdot\boldsymbol{f}^T$ is represented by a 2×2 matrix on account of symmetry properties of the bulk.

To locate the chemical potential $\mu^{\alpha\beta}$ at which (metastable or stable) phases α and β (represented by $\boldsymbol{x}^\alpha$ and $\boldsymbol{x}^\beta$, respectively) coexist we expand ω in a Taylor series

$$\begin{aligned}\omega(\mu,\boldsymbol{x})&=\omega(\mu_i,\boldsymbol{x})+\left.\frac{d\omega}{d\mu}\right|_{\mu=\mu_i,\boldsymbol{x}}(\mu-\mu_i)+O((\mu-\mu_i)^2)\\ &\simeq\omega(\mu_i,\boldsymbol{x})-\overline{\rho}_i(\mu-\mu_i),\end{aligned} \tag{3.8}$$

which we truncate after the linear term. In Eq. (3.8), $\overline{\rho}_i$ is the mean pore density defined in Eq. (2.19).The chemical potential at coexistence is then estimated by solving

$$\omega(\mu^{\alpha\beta},\boldsymbol{x}^\alpha)=\omega(\mu^{\alpha\beta},\boldsymbol{x}^\beta), \tag{3.9}$$

for $\mu^{\alpha\beta}$. From Eq. (3.8) and (3.9), we obtain an improved estimate for the chemical potential at coexistence from

$$\mu_{i+1}^{\alpha\beta}=\frac{\omega(\mu_i^{\alpha\beta},\boldsymbol{x}_i^\beta)-\omega(\mu_i^{\alpha\beta},\boldsymbol{x}_i^\alpha)}{\overline{\rho}_i^\beta-\overline{\rho}_i^\alpha}+\mu_i^{\alpha\beta}, \tag{3.10}$$

where $\boldsymbol{x}_i^\alpha$, $\boldsymbol{x}_i^\beta$, $\overline{\rho}_i^\alpha$, and $\overline{\rho}_i^\beta$ are obtained from the final solutions of Eq. (3.7) for $\mu_i=\mu$ [see Eq. (3.5b)]. However, for $\mu_{i+1}^{\alpha\beta}$, $\boldsymbol{x}_i^\alpha$, and $\boldsymbol{x}_i^\beta$ no longer satisfy Eq. (3.4). Hence, we replace in Eq. (3.5b), μ_0 by μ_i and $\delta\mu$ by $\delta\mu=\mu_{i+1}-\mu_i$, solve Eq. (3.4) for $\boldsymbol{x}^\alpha$ and $\boldsymbol{x}^\beta$, and repeat the scheme just described until $|\delta\mu|\leqslant 10^{-11}$. Finally, we return to Eq. (3.5a) until the relevant temperature range has been covered.

IV. RESULTS

A. Phase diagram of binary bulk mixtures

We begin the discussion with bulk mixtures for which we display in Fig. 1 characteristic phase diagrams for selected values of ϵ_{AB}. Henceforth, all quantities are expressed in the customary dimensionless (i.e., ''reduced'') units. That is, energies are given in units of ϵ, temperature in units of $|\epsilon|/k_B$ ($\epsilon \leqslant 0$). To realize a binary bulk mixture, we choose $\epsilon_W = 0$, $z=1$ in Eqs. (A3), (A4), and (A6), and replace the hard-substrate boundary conditions $\rho_0 = \rho_{z+1} = 0$ by periodic boundary conditions $\rho_0 = \rho_{z+1} = \rho_1$ to account for the symmetry of the bulk mixture. Equation (A6) is used in the limit $T=0$ which serves to provide suitable starting solutions for the iterative procedure detailed in Sec. III B.

Results plotted in Fig. 1 for various values of ϵ_{AB} illustrate generic types of phase diagrams defined as the union

$$\mu_x(T) \equiv \cup_{\alpha,\beta} \mu_x^{\alpha\beta}(T) \tag{4.1}$$

of coexistence lines $\mu_x^{\alpha\beta}(T)$ between pairs of phases α and β. Bulk phase diagrams have also been discussed earlier by Wilding *et al.* [35]. These authors studied the phase behavior of a *continuous* square-well binary bulk mixture by means of Monte Carlo simulations and a mean-field approach. For $\epsilon_{AB}=0.40$ plots in Fig. 1(a) show that for temperatures $T \lesssim 1.32$ only gas and demixed liquid coexist along a line of first-order phase transitions. This line ends at a tricritical point located at $\mu_{\rm tri} \simeq -1.75$ and $T_{\rm tri} \simeq 1.32$. For temperatures exceeding $T_{\rm tri}$, gas and demixed liquid coexist along the so-called λ line [i.e., a line of critical points indicated by the thin solid line in Fig. 1(a)]. This type of phase diagram resembles the one shown by Wilding *et al.* in their Fig. 1(c) [35].

For higher $\epsilon_{AB}=0.5$ the phase diagram differs qualitatively from the previous one. This can be seen from Fig. 1(b) where a bifurcation appears (i.e., at a triple point) for $\mu_{\rm tr} \simeq -2.25$ and $T_{\rm tr} \simeq 1.075$ at which a gas phase coexists simultaneously with both a mixed and a demixed fluid phase. Consequently a critical point exists ($\mu_c \simeq -2.25, T_c \simeq 1.15$) at which the line of first-order transitions between mixed liquid and gas states ends. The line of first-order transitions involving mixed and demixed liquid states ends at a higher temperature and chemical potential of $\mu_{\rm tri} \simeq -2.00$ and $T_{\rm tri} \simeq 1.18$ and the λ line is shifted towards lower temperatures as one can see from the plot in Fig. 1(b). This type of phase diagram comports with the one shown in Fig. 1(b) of Wilding *et al.* [35].

A further slight increase of ϵ_{AB} to 0.56 does not cause the phase diagram to change *qualitatively* but *quantitatively* from the previously discussed case. This can be seen in Fig. 1(c), where for $\epsilon_{AB}=0.56$ the triple point is shifted to a lower temperature and chemical potential compared with $\epsilon_{AB}=0.50$. Likewise, the line of first-order transitions between gas and mixed liquid appears at lower chemical potential but is somewhat longer since the critical point is elevated to a higher $T_c \simeq 1.18$. The opposite is true for the coexistence between mixed and demixed liquid phases as one can see from Figs. 1(b) and 1(c).

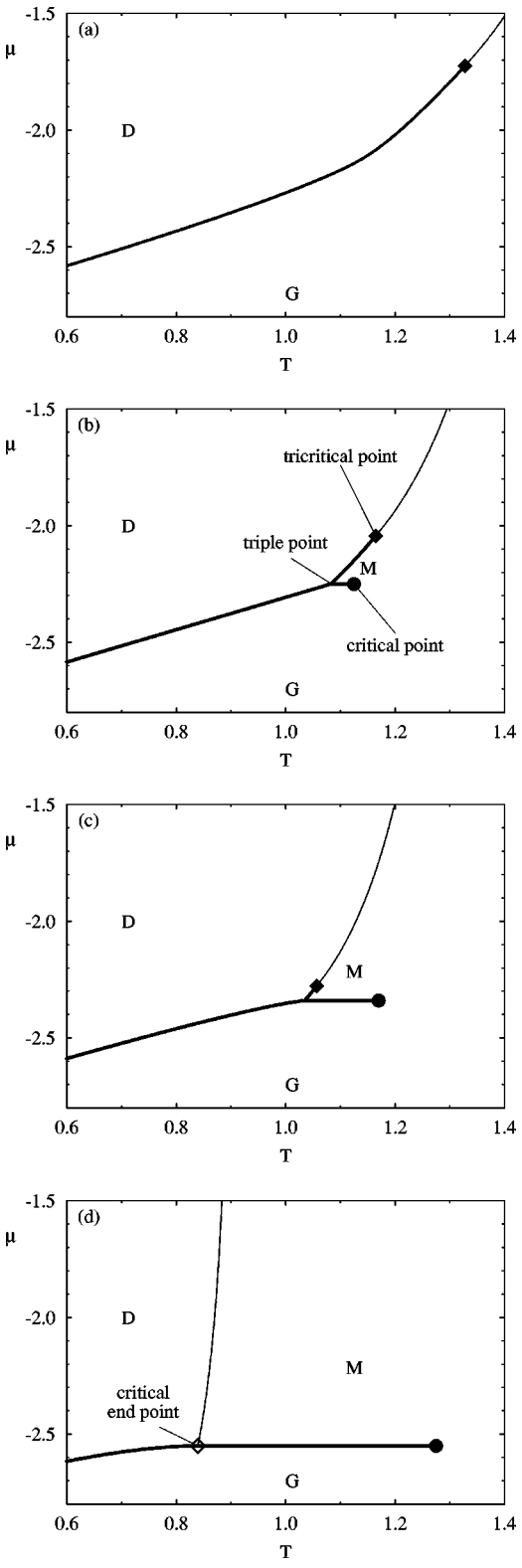

FIG. 1. Bulk phase diagrams $\mu_x(T)$ [see Eq. (4.1)], where *G*, *M*, and *D* refer to one-phase regions of gaseous, mixed liquid, and demixed liquid phases, respectively. Pairs of neighboring phases coexist for state points represented by solid lines where thick and thin lines refer to first-order and second-order phase transitions, respectively. (a) $\epsilon_{AB}=0.40$, (b) $\epsilon_{AB}=0.50$, (c) $\epsilon_{AB}=0.56$, (d) $\epsilon_{AB}=0.70$.

Eventually, as ϵ_{AB} becomes sufficiently large, first-order transitions between mixed and demixed liquid phases disappear as the plot in Fig. 1(d) shows. For $\epsilon=0.70$ the λ line intersects a line of first-order phase transitions at a critical end point $\mu_{\mathrm{CEP}}\simeq-2.55$, $T_{\mathrm{CEP}}\simeq0.84$ since the nature of the participating phases along the λ line differs from those involved in the first-order transitions for $T<T_{\mathrm{CEP}}$ or $T>T_{\mathrm{CEP}}$. This type of phase diagram resembles the one plotted in Fig. 1(a) in the paper of Wilding *et al.* [35].

In the limit $\epsilon_{AB}=1.0$ the symmetric binary mixture degenerates to a pure fluid. In this case $T_{\mathrm{CEP}}\to0$ and the λ line becomes formally indistinguishable from the μ axis (and therefore physically meaningless). The remaining coexistence line $\mu_{\mathrm{x}}^{GL}=-3=\mu_{\mathrm{x}}$ (i.e., the phase diagram) involving gas (G) and liquid phases (L) becomes parallel with the T axis and ends at the critical point where $T_{\mathrm{c}}=\frac{3}{2}$ ($\mu_{\mathrm{c}}=-3$) as expected for the bulk lattice gas [36] (see, for example, Fig. 9 in Ref. [37]).

B. Phase behavior of confined binary mixtures

If a fluid is confined to spaces of molecular dimension(s) one expects their phase behavior to be altered from that of their bulk counterpart in several significant ways. For example, as far as pure fluids are concerned experiments [38] and theoretical approaches [32] have repeatedly demonstrated that the gas-liquid critical point is shifted to lower critical temperatures and higher (average) densities of the confined fluid. The effect is more pronounced the more severely confined the fluid is (i.e., the smaller the pore width is).

In a confined binary mixture a similar confinement-induced shift of the critical point is observed. This is apparent from plots in Fig. 2 where the critical point involving gas and mixed liquid phase is shifted to progressively lower T and μ with decreasing pore width z. For the present value of $\epsilon_{AB}=0.6$ the phase diagram of the confined fluid corresponds to type III [see Fig. 2(a)] illustrated by the plot of the bulk analog shown in Fig. 1(d). Another confinement effect, that does not have any counterpart in pure fluids, can also be seen from Fig. 2. It concerns a downward shift of the tricritical point $\{T_{\mathrm{tri}},\mu_{\mathrm{tri}}\}$ with increasing degree of confinement (i.e., as z becomes smaller).

For a given substrate separation z and $\epsilon_{AB}=0.6$ the strength of the fluid-substrate interaction ϵ_W also has profound consequences for both T_{c} and T_{CEP} as plots in Fig. 2 show. From Fig. 2(b), it is obvious that increasing ϵ_W causes a depression of T_{c} for a given value of z. The effect increases with decreasing width of the slit pore. The depression of T_{c} can be understood in terms of enhanced gas adsorption at the substrate surfaces with increasing ϵ_W. Thus, for a given T the mean densities of coexisting gas and mixed liquid phases are less different the larger ϵ_W becomes. Consequently, T_{c}, at which the two become identical by definition, decreases with increasing fluid-substrate attraction (while holding z constant).

A similar confinement effect is observed for the critical-end-point temperature in Fig. 2(c). Like T_{c}, T_{CEP} first decreases with ϵ_W for each given z [see curves for $\epsilon_W=0.7$, 1.0 in Fig. 2(c)]. However, for larger $\epsilon_W\geqslant1.0$, T_{CEP} increases with the strength of the fluid-substrate attraction. Both trends can be understood in terms of a competition between entropic versus energetic effects as we shall discuss below in Sec. V. The increase of T_{CEP} with ϵ_W reflects enhanced decomposition of the confined fluid since a higher T_{CEP} reduces the size of the one-phase region of mixed fluid phases relative to the one-phase region of demixed states. However, compared with the confinement-induced shift of T_{c} the impact of varying ϵ_W is quite small for T_{CEP}. It is furthermore gratifying that the confinement-induced depression of T_{c} and T_{CEP} diminishes rather quickly as $z\to\infty$ so that a smooth extrapolation of our results to the bulk limit is achieved.

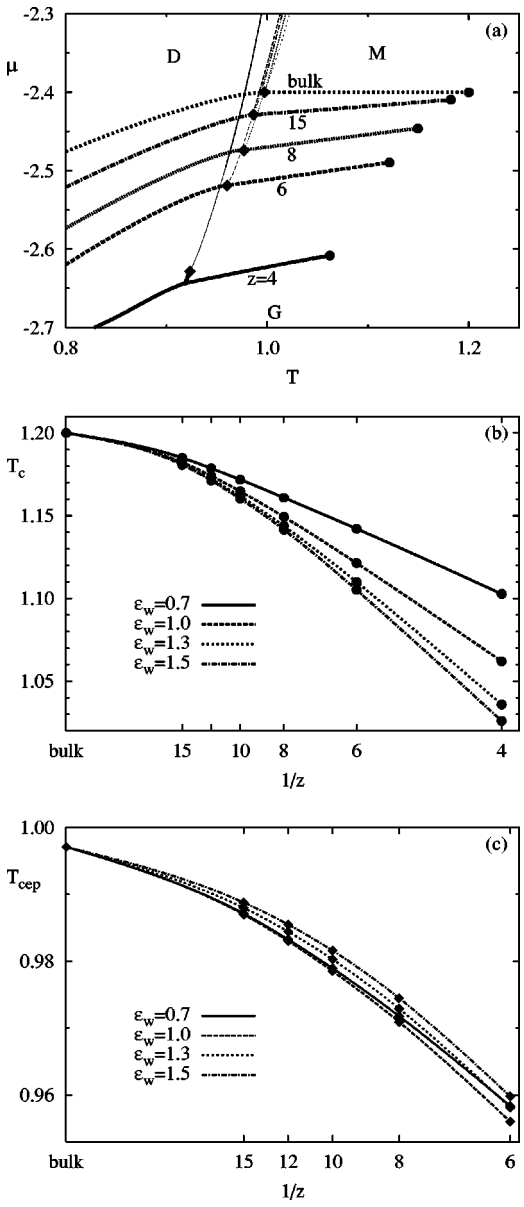

FIG. 2. (a) As Fig. 1, but for various degrees of confinement (i.e., z) indicated in the figure where (♦) denote the tricritical and (●) the critical point, respectively ($\epsilon_{AB}=0.6,\epsilon_W=1.0$); (b) critical temperature T_{c} versus inverse pore width for various values of ϵ_W indicated in the figure; (c) as (b), but for critical-end-point temperature T_{CEP}.

If, on the other hand, a smaller $\epsilon_{AB}=0.4$ is concerned, a thermodynamically stable mixed liquid phase is absent and we are dealing with a phase diagram of type I [see Fig. 1(a)]. If the fluid-substrate interaction is weakly attractive [$\epsilon_W=0.1$, see Fig. 3(a)], a *gaseous* phase coexists with a dense demixed *liquid* phase up to the tricritical point where the two become indistinguishable.

However, for a larger fluid-substrate attraction $\epsilon_W=1.15$ the plot in Fig. 3(b) exhibits a bifurcation at the triple point $\mu_{\rm tr}\simeq-2.47$, $T_{\rm tr}\simeq0.87$. For $T\leqslant T_{\rm tr}$ gas coexists with a demixed film of finite thickness adsorbed on either substrate, whereas for $T>T_{\rm tr}$ gas still coexists with demixed fluid along the respective coexistence lines $\mu_{\rm x}^{GDF}(T)$ and $\mu_{\rm x}^{GD}(T)$ in Fig. 3(b). The demixed film eventually undergoes capillary condensation to a demixed fluid if $\mu>\mu_{\rm x}^{DFD}(T)$ along an isotherm $T<T_{\rm tr}$. Thus, as shown in Fig. 3(b) the demixed wetting film is thermodynamically stable over a narrow range of chemical potentials.

If ϵ_W increases further to a value of 1.3 [see Fig. 3(c)], say, the triple point of gas, demixed film, and demixed fluid disappears. Instead a second tricritical point appears at $\mu_{\rm tri}\simeq-2.52$, $T_{\rm tri}\simeq0.91$ involving gas and demixed film. At this triple point a λ line appears which intersects the coexistence line between demixed fluid and the (now indistinguishable) gas and demixed film at the critical end point $\mu_{\rm CEP}\simeq-2.30$, $T_{\rm CEP}\simeq1.02$. For $T>T_{\rm CEP}$ gas and demixed fluid coexist for thermodynamic states represented by the thick solid line in Fig. 3(c). These latter phases become indistinguishable at the tricritical point $\mu_{\rm tri}\simeq-1.92$, $T_{\rm tri}\simeq1.26$ where a second λ line begins.

For even larger $\epsilon_W=3.0$ the plot in Fig. 3(d) indicates that the critical end point has disappeared. The coexistence line between gas and demixed film is shifted to lower chemical potentials ending at a tricritical point where a λ line starts that does no longer intersect the line of first-order transitions between a demixed film and the demixed fluid. This line now ends at a true critical point $\mu_{\rm c}\simeq-2.00$, $T_{\rm c}\simeq1.23$ where the latter two become indistinguishable. To verify that the the point $\mu_{\rm c}\simeq-2.00$, $T_{\rm c}\simeq1.23$ is a legitimate critical point we numerically analyzed the order parameter $\overline{\rho}^{D}-\overline{\rho}^{DF}$ which follows a scaling law $(1-T/T_{\rm c})^{\beta}$ as $T\to T_{\rm c}^{-}$. As expected our analysis gives the mean-field value $\beta\simeq\frac{1}{2}$ for the critical exponent.

C. Confinement-controlled decomposition of binary mixtures

In the preceding Sec. IV B system parameters were chosen such that the type of the phase diagram remained unaltered upon a variation of one or more of these parameters. However, by varying the degree of confinement (i.e., z) it is also possible to switch between various types of phase diagrams with profound consequences for liquid-liquid and gas-liquid phase equilibria which may have practical implications for the decomposition of mixtures of immiscible liquids.

Consider as an example the case $\epsilon_{AB}=0.5$ for which the bulk phase diagram is plotted in Fig. 4(a). It consists of a line of first-order phase transitions involving gaseous and demixed liquid states for $T\lesssim1.08$. At $T_{\rm tr}\simeq1.08$ the phase diagram bifurcates into a line of first-order phase transitions between gaseous and mixed liquid states ending at the critical point $\mu_{\rm c}\simeq-2.25$, $T_{\rm c}\simeq1.13$ and a line of first-order transitions involving mixed and demixed liquid states. The latter

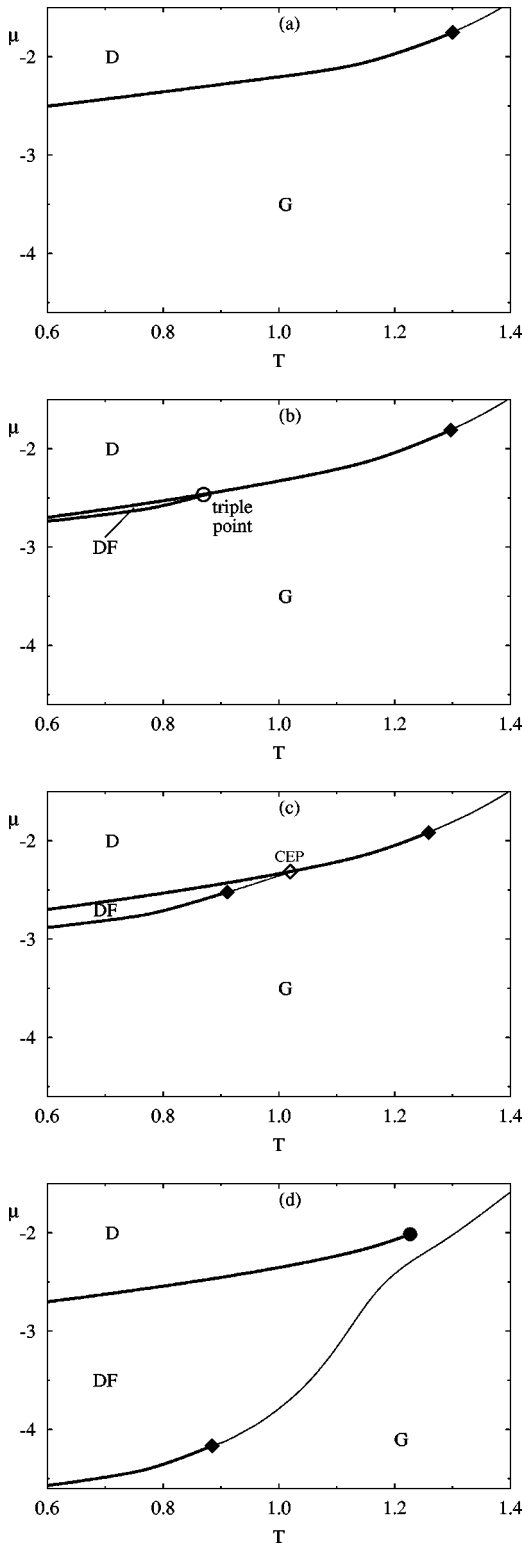

FIG. 3. As Fig. 1 but for various strengths of fluid-substrate attraction, $\epsilon_{AB}=0.4$, and $z=10$. (a) $\epsilon_W=0.10$, (b) $\epsilon_W=1.15$, (c) $\epsilon_W=1.30$, (d) $\epsilon_W=3.00$.

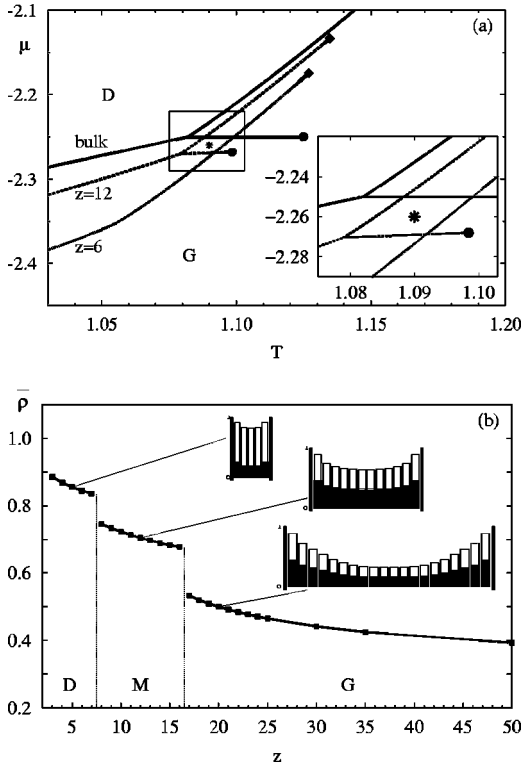

FIG. 4. (a) As Fig. 1, where the inset is an enhanced representation of that part of the phase diagrams bounded by the box with a fixed thermodynamic state represented by *. (b) Mean pore density $\bar{\rho}$ as a function of pore width z where stability limits between pairs of phases are demarcated by vertical lines; also shown are histograms of the local density of representative phases where the shading of the bars refers to ρ_l^A and ρ_l^B, respectively.

ends at the tricritical point $\mu_{\mathrm{tri}} \simeq -2.04$ and $T_{\mathrm{tri}} \simeq 1.16$. Hence, for the present choice of model parameters the bulk phase diagram is of type II [see Figs. 1(b) and 1(c)]. If this binary mixture is now confined to a relatively wide slit pore, the phase diagram remains of type II but the plot referring to $z=12$ in Fig. 4(a) clearly shows the confinement-induced downward shift of coexistence lines and the displacement of characteristic (i.e., triple, critical, and tricritical) points discussed in the preceding section. However, if the degree of confinement becomes more severe [see plot for $z=6$ in Fig. 4(a)] the character of the phase diagram changes from type II to I according to the classification scheme developed on the basis of Figs. 1(b) and 1(a), respectively. In other words, by going from $z=12$ to $z=6$ the mixed liquid vanishes as a thermodynamically stable phase, while the entire phase diagram is further shifted to lower chemical potentials. This latter trend persists if the pore width is reduced even more with no further change in the type of phase diagram.

If one then fixes the thermodynamic state such that the bulk mixture is a gas [represented by $*$ in the inset in Fig. 4(a)], confinement to a relatively wide pore (i.e., $z=12$) may first cause capillary condensation to a mixed liquid mixture analogous to ordinary capillary condensation in pure fluids. If the fluid is confined to a narrower pore ($z=6$), however, decomposition into *A*-rich and *B*-rich liquid phases is triggered by confinement upon condensation. Thus, by choosing an appropriate pore width one can either promote condensation of a gas to a mixed liquid phase or, alternatively, initiate liquid-liquid phase separation in the porous matrix where both processes are solely confinement driven since the pore walls are nonselective for molecules of either species in our present model.

This process is further illustrated by the plots in Fig. 4(b) where the mean density $\bar{\rho}$ of thermodynamically stable confined phases is plotted as a function of z (i.e., the pore width). Three different branches are discernible. For small $z<8$, $\bar{\rho}$ is relatively high indicating that the pore is filled with liquid. A corresponding plot of the local densities of a representative phase for $z=5$ shows that this liquid consists locally of *A*- (or *B*-)rich, high-density fluid (since the two cannot be distinguished in a symmetric mixture). Hence, for $z<8$ we observe (local) decomposition of liquid mixtures. Along an intermediate branch of pore widths, that is, for $8<z<16$, $\bar{\rho}$ is somewhat smaller than for the tightest pores ($z<8$). An inspection of a prototypical plot of the local densities for $z=12$ reveals that the confined phase now consists of a locally equimolar mixture. Hence, for intermediate pore sizes the confined phase is a mixed liquid. Finally, for $z>16$, $\bar{\rho}$ is still smaller than along the two previously discussed branches. The local density of a representative state for $z=20$ now clearly shows that a comparatively low-density fluid exists at the center of the pore. As either substrate is approached the density increases indicating that this mixture wets the substrates. However, as expected for such a ''gas'' state the fluid is composed locally of an equimolar mixture similar to states along the intermediate branch $8<z<16$. The change of $\bar{\rho}$ between a pair of branches is discontinuous at characteristic pore widths where the first-order transitions occur between these phases.

V. SUMMARY AND CONCLUSIONS

In this work, we investigate the phase behavior of a symmetric binary mixture confined to slit pores with chemically homogeneous, planar substrate surfaces. The substrates are nonselective, that is, the strength of the fluid-substrate interaction for molecules of component *A* is identical to that for molecules of component *B*. The dimensionality of configuration space is reduced by restricting positions of fluid molecules to sites on a simple-cubic lattice. Moreover, the interaction between fluid molecules and between a fluid molecule and the substrates is governed by square-well potentials where the widths of the attractive wells is chosen such that only nearest-neighbor interactions are accounted for.

In addition to discretization, we employ a mean-field approximation to the Hamiltonian governing our lattice-gas model which is expected to be sufficiently realistic for our present purposes [34]. When it comes to fluid (i.e., gas or liquid) phases, discretization of configuration space might seem somewhat problematic at first sight. However, lattice models have been employed frequently to investigate generic features of fluid phases in the past even if much more complex polymeric systems are considered [34,39,40]. Perhaps

the greatest advantage of mean-field lattice-gas models is that they permit to calculate entire phase diagrams with comparably little computational effort even for rather complex model systems [33,41]. This aspect is particularly important in the context of this work where the parameter space, on which our model is defined, is rather highly dimensional.

To reduce the dimensionality of the parameter space we restrict this study to symmetric binary mixtures characterized by $\epsilon_{AA}=\epsilon_{BB}$, thus permitting only the cross interaction between molecules of species A and B to vary in order to promote either mixing ($\epsilon_{AB}>1$) or decomposition ($\epsilon_{AB}<1$). Moreover, we fix $\mu_A=\mu_B$ to reduce the number of relevant model parameters even further.

Based upon a modular approach introduced by Bock *et al.* [33], we can then determine the complete set of phases (i.e., occupation-number patterns) of the binary mixture at $T=0$. These phases serve as suitable starting solutions for the numerical minimization of the grand potential for $T>0$, which eventually permits us to determine complete phase diagrams of bulk and confined binary mixtures over the entire temperature range (see Sec. III).

By varying ϵ_{AB}, we determine essentially three different generic types of bulk phase diagrams. In mixtures pertaining to type I, (mixed) gas and demixed liquid mixtures coexist along a line of first-order phase transitions up to the tricritical point at which the transition between these two phases becomes second order for all $T\geqslant T_{\mathrm{tri}}$ (i.e., along the so-called λ line). A mixed liquid does not occur as a thermodynamically stable phase due to the relatively low value of ϵ_{AB} characteristic of mixtures of type I [see Fig. 1(a)].

For intermediate values of ϵ_{AB} the phase diagram is of type II where now a mixed liquid arises as a third thermodynamically stable phase. In mixtures of type II, this mixed liquid may coexist with either demixed liquid or gas phases independently. Thus, besides a tricritical point involving now mixed and demixed liquid phases, a critical point exists at which gaseous and mixed liquid phases become indistinguishable [see Fig. 1(b)].

A third type of phase diagrams exists for sufficiently large values of ϵ_{AB}. Phase diagrams of type III are characterized by the existence of gaseous, mixed, and demixed liquids as thermodynamically stable phases. However, lines of first-order phase transitions exist only between gas and demixed liquid on one hand and gas and mixed liquid on the other hand; the transition between mixed and demixed liquid phases is always second order along the λ line [see Fig. 1(d)]. The λ line now terminates at a critical end point where it meets the lines of first-order transitions $\mu_{\mathrm{x}}^{GD}(T)$ and $\mu_{\mathrm{x}}^{GM}(T)$.

The three types of phase diagrams for symmetric binary bulk mixtures comport qualitatively with the general classification scheme proposed earlier by Wilding *et al.* for a related model [35]. Since these authors employed a continuous model, quantitative differences between their and our phase diagrams are inevitable. More important, however, is the qualitative agreement between the results obtained by Wilding *et al.* and us, since it allows us to conclude that the general features of phase diagrams of type I–III are indeed generic, that is, model-independent, as far as symmetric binary mixtures of simple fluids are concerned.

In the context of confined binary mixtures, we focus on a variation of both the degree of confinement (i.e., the width of the slit pore z) and the ''wettability'' of the substrates (i.e., the strength of the fluid-substrate interaction ϵ_W) disregarding deliberately a detailed discussion of wetting phenomena to which we shall turn our attention in a separate publication [42]. Generally speaking, confinement causes a depression of both critical and critical-end-point temperatures provided ϵ_W is large enough for the latter to exist [see Fig. 3(a)]. In this case varying ϵ_W for fixed pore width z causes an additional depression of T_{c} [see Fig. 2(b)]; the opposite but much smaller trend is observed for T_{CEP} with increasing ϵ_W at fixed z [see Fig. 2(c)]. Both effects seem plausible if one realizes that the mean density of the gas phase in coexistence with a mixed liquid phase increases on account of more pronounced adsorption of the gas at the substrate for larger ϵ_W. In other words, the larger ϵ_W the lower the temperature T_{c} at which gas and mixed liquid phase become indistinguishable. Likewise, at the critical end point, mixed and demixed liquid phases are indistinguishable from gaseous phases of a density increasing with ϵ_W. Since the pore wall is nonselective for either component and because of our present choice of $\epsilon_{AB}=0.6$, which promotes decomposition, it seems obvious that the stronger the substrate attracts fluid molecules the larger is the tendency of the confined mixture to decompose as reflected by a somewhat larger T_{tri}. This is because once a molecule of either component is adsorbed by the pore wall it is energetically more favorable to surround it by other like molecules. Entropically, the opposite would be true which means that for the present choice of parameters properties of the confined phase are controlled by energetic rather than entropic effects. This is no longer so if $\epsilon_W=0.7$ where T_{CEP} for a given value of z is intermediate to the curves pertaining to $\epsilon_W=1.0$ and $\epsilon_W=1.3$ and in Fig. 2(c). In this case, attraction by the walls is too weak and the entropic effects ''win'' over the energetic ones so that the walls now favor mixing of the two components rather than decomposition. However, the effects are rather small as a comparison of Figs. 2(b) and 2(c) shows.

Another, more significant finding concerns strong fluid-substrate attraction and is illustrated by the plot in Fig. 3(d) where $\mu_{\mathrm{x}}^{DFD}(T)$ ends at a true critical point. This is remarkable because the (mean) density of the demixed film (DF) adsorbed on the substrates is relatively low so that ordinarily one would anticipate a thermodynamically stable mixed phase. This phenomenon, to the best of our knowledge, has not been reported previously.

Perhaps the most significant finding of the present work concerns confinement-induced changes in the type of phase diagram describing the confined fluid mixture. As illustrated in Fig. 4 by varying z for fixed and suitably chosen values of ϵ_{AB} and ϵ_W it is not only possible to shift all coexistence lines to lower μ but also to switch from a phase diagram of type II to one of type I, that is to eliminate mixed liquids as thermodynamically stable phases (see Fig. 4). This may have important repercussions for the decomposition of binary mixtures in sorption experiments where one may envision pore condensation in nanoscopic solid matrices leading ei-

ther to a mixed or demixed liquid phase depending solely on the pore width.

ACKNOWLEDGMENT

We are grateful to the Sonderforschungsbereich 448 ''Mesoskopisch strukturierte Verbundsysteme'' for financial support.

APPENDIX A: DERIVATION OF EQS. (2.18)

An explicit expression for ω is obtained by inserting Eqs. (2.10) and (2.14) into Eq. (2.16) which yields

$$\begin{aligned}\omega(T,\mu)=&-\frac{1}{\beta z}\sum_{l=1}^{z}\Bigg[-\rho_l\ln\rho_l-(1-\rho_l)\ln(1-\rho_l)+\rho_l\ln 2\\&-\frac{\rho_l}{2}\{(1+m_l)\ln(1+m_l)+(1-m_l)\ln(1-m_l)\}\Bigg]\\&+\frac{1}{z}\sum_{l=1}^{z}\rho_l\Bigg[\frac{\epsilon}{4}\{\rho_{l+1}(1+m_lm_{l+1})+\rho_{l-1}\\&\times(1+m_lm_{l-1})+4\rho_l(1+m_l^2)\}\\&+\frac{\epsilon_{AB}}{4}\{\rho_{l+1}(1-m_lm_{l+1})+\rho_{l-1}(1-m_lm_{l-1})\\&+4\rho_l(1-m_l^2)\}\Bigg]-\frac{1}{z}\sum_{l=1}^{z}\rho_l\mu+\frac{\epsilon_W}{z}(\rho_1+\rho_z).\end{aligned}\tag{A1}$$

Employing Eq. (A1) in Eq. (2.18) a set of $2z$ coupled transcendental equations, namely,

$$0=\frac{1}{2\beta}\ln\frac{1+m_l}{1-m_l}+\frac{\epsilon-\epsilon_{AB}}{2}(\rho_{l+1}m_{l+1}+\rho_{l-1}m_{l-1}+4\rho_lm_l),\tag{A2a}$$

$$\begin{aligned}\overline{\mu}\equiv\mu+\beta^{-1}\ln 2=&\beta^{-1}\Bigg[\ln\frac{\rho_l}{1-\rho_l}+\frac{1}{2}\{(1+m_l)\ln(1+m_l)\\&+(1-m_l)\ln(1-m_l)\}\Bigg]+\frac{\epsilon+\epsilon_{AB}}{2}(\rho_{l+1}+\rho_{l-1}+4\rho_l)\\&+\frac{\epsilon-\epsilon_{AB}}{2}m_l(\rho_{l+1}m_{l+1}+\rho_{l-1}m_{l-1}+4\rho_lm_l)\\&+\epsilon_W(\delta_{1l}+\delta_{zl}),\end{aligned}\tag{A2b}$$

is obtained after somewhat lengthy but straightforward algebra where δ_{ij} denotes the Kronecker symbol. We can solve Eqs. (A2) by first reorganizing Eq. (A2b) such that

$$\begin{aligned}&\rho_{l+1}\frac{\epsilon+\epsilon_{AB}}{2}-m_lm_{l+1}\rho_{l+1}\frac{\epsilon_{AB}-\epsilon}{2}\\&=\overline{\mu}-\beta^{-1}\Bigg[\ln\frac{\rho_l}{1-\rho_l}+\frac{1}{2}\{(1+m_l)\ln(1+m_l)\\&+(1-m_l)\ln(1-m_l)\}\Bigg]-\frac{\epsilon+\epsilon_{AB}}{2}(\rho_{l-1}+4\rho_l)\\&+\frac{\epsilon_{AB}-\epsilon}{2}m_l(\rho_{l-1}m_{l-1}+4\rho_lm_l)+\epsilon_W(\delta_{1l}+\delta_{zl}).\end{aligned}\tag{A3}$$

Likewise, we may rewrite Eq. (A2a) as

$$\begin{aligned}\rho_{l+1}m_{l+1}+\rho_{l-1}m_{l-1}=&-\frac{1}{\beta(\epsilon-\epsilon_{AB})}\ln\frac{1+m_l}{1-m_l}-4\rho_lm_l\\\equiv&\,g_2(\rho_l,m_l).\end{aligned}\tag{A4}$$

Inserting now Eq. (A4) into Eq. (A3), we eventually obtain

$$\begin{aligned}\rho_{l+1}+\rho_{l-1}=&\frac{2\overline{\mu}}{\epsilon+\epsilon_{AB}}-\frac{2}{\beta(\epsilon+\epsilon_{AB})}\Bigg[\ln\frac{\rho_l}{1-\rho_l}-\frac{m_l}{2}\ln\frac{1+m_l}{1-m_l}\\&+\frac{1}{2}\{(1+m_l)\ln(1+m_l)+(1-m_l)\ln(1-m_l)\}\Bigg]\\&-4\rho_l-\frac{2\epsilon_W}{\epsilon+\epsilon_{AB}}(\delta_{1l}+\delta_{zl})\equiv g_1(\rho_l,m_l).\end{aligned}\tag{A5}$$

Note that both ρ_l and m_l are continuous on the intervals $[0,1]$ and $[-1,1]$, respectively.

In the limit of vanishing temperature ($1/\beta=0$), on the other hand, entropic contributions to ω vanish and one has from Eq. (A1)

$$\begin{aligned}\omega(0,\mu)=&\frac{1}{z}\sum_{l=1}^{z}\rho_l\Bigg[\frac{\epsilon}{4}\{\rho_{l+1}(1+m_lm_{l+1})\\&+\rho_{l-1}(1+m_lm_{l-1})+4\rho_l(1+m_l^2)\}\\&+\frac{\epsilon_{AB}}{4}\{\rho_{l+1}(1-m_lm_{l+1})+\rho_{l-1}(1-m_lm_{l-1})\\&+4\rho_l(1-m_l^2)\}\Bigg]-\frac{1}{z}\Bigg[\sum_{l=1}^{z}\rho_l\mu-\epsilon_W(\rho_1+\rho_z)\Bigg],\end{aligned}\tag{A6}$$

where the mean density at $T=0$, $\rho_l=0,1$ is a double-valued discrete quantity since a given plane l can only be occupied or empty. For $\rho_l=0$, $m_l=0$ is the only sensible possibility. If, on the other hand, $\rho_l=1$, $m_l=0,\pm1$ is triple-valued depending on whether this particular site is occupied by an equimolar mixed liquid ($m_l=0$), pure component A ($m_l=1$), or pure component B ($m_l=-1$).

[1] L.D. Gelb, K.E. Gubbins, R. Radhakrishnan, and M. Sliwinska-Bartkowiak, Rep. Prog. Phys. **62**, 1573 (1999).
[2] L.V. Entov, V.A. Levchenko, and V.P. Voronov, Int. J. Thermophys. **14**, 221 (1993).
[3] V.P. Voronov and V.M. Buleiko, J. Esp. Theor. Phys. **86**, 586 (1998).
[4] M. Sliwinska-Bartkowiak, R. Sikorski, S.L. Sowers, L.D. Gelb, and K.E. Gubbins, Fluid Phase Equilib. **136**, 93 (1997).
[5] W.I. Goldburg, F. Aliev, and X.-I. Wu, Physica A **213**, 61 (1995).
[6] M.Y. Lin, S.K. Sinha, J.M. Drake, X.-I. Wu, P. Thiyagarajan, and H.B. Stanley, Phys. Rev. Lett. **72**, 2207 (1994).
[7] D.J. Tulimieri, J. Yoon, and M.H.W. Chan, Phys. Rev. Lett. **82**, 121 (1999).
[8] F. Formisano and J. Teixeira, Eur. Phys. J. E **1**, 1 (2000).
[9] J.V. Maher, W.I. Goldburg, D.W. Pohl, and M. Lanz, Phys. Rev. Lett. **53**, 60 (1984).
[10] B.J. Frisken, D.S. Cannell, M.Y. Lin, and S.K. Sinha, Phys. Rev. E **51**, 5866 (1995).
[11] B.J. Frisken, F. Ferri, and D.S. Cannell, Phys. Rev. E **51**, 5922 (1995).
[12] Z. Zhuang, A.G. Casielles, and D.S. Cannell, Phys. Rev. Lett. **77**, 2969 (1996).
[13] M. Müller and W. Paul, J. Stat. Phys. **93**, 209 (1997).
[14] J.C. Lee, Phys. Rev. Lett. **70**, 3599 (1993).
[15] H.L. Frisch, S. Puri, and P. Nielaba, J. Chem. Phys. **110**, 10514 (1999).
[16] T. MacFarland, G. Barkema, and J.F. Marko, Phys. Rev. B **53**, 148 (1996).
[17] M. Kotelyanskii and S.K. Kumar, Phys. Rev. Lett. **80**, 1252 (1998).
[18] P. Keblinski, W.-J. Ma, A. Maritan, J. Koplik, and J.R. Banavar, Phys. Rev. E **47**, R2265 (1993).
[19] Z. Zhang and A. Chakrabarti, Phys. Rev. E **52**, 2736 (1995).
[20] L.D. Gelb and K.E. Gubbins, Phys. Rev. E **56**, 3185 (1997).
[21] W.T. Gozdz, K.E. Gubbins, and A.Z. Panagiotopoulos, Mol. Phys. **84**, 825 (1995).
[22] J.E. Curry and J.H. Cushman, Mol. Phys. **85**, 173 (1995).
[23] J.E. Curry and J.H. Cushman, J. Chem. Phys. **103**, 2132 (1995).
[24] K. Grabowski, A. Patrykiejew, and S. Sokolowski, Thin Solid Films **379**, 297 (2000).
[25] E. Kierlik, Y. Fan, P.A. Monson, and M.L. Rosinberg, J. Chem. Phys. **102**, 3712 (1994).
[26] O. Pizio, A. Patrykiejew, and S. Sokolowski, Mol. Phys. **99**, 57 (2001).
[27] A. Trokhymchuk, O. Pizio, S. Sokolowski, and D. Henderson, Mol. Phys. **86**, 53 (1995).
[28] E. Schöll–Paschinger, D. Levesque, J.-J. Weis, and G. Kahl, Phys. Rev. E **64**, 011502 (2001).
[29] M. Müller, Macromol. Theory Simul. **8**, 343 (1999).
[30] K. Binder, M. Müller, and E.V. Albano, Phys. Chem. Chem. Phys. **3**, 1160 (2001).
[31] M. Grün, K. K. Unger, A. Matsumoto, and K. Tsutsumi, *Characterization of Porous Solids*, edited by B. McEnaney, T. J. Mays, J. Roquérol, F. Rodriguez-Reinoso, K. S. W. Sing, and K. K. Unger (The Royal Society of Chemistry, Cambridge, 1997), Vol. IV, p. 81.
[32] A. Schreiber, H. Bock, M. Schoen, and G. H. Findenegg, Mol. Phys. **100**, 2097 (2002).
[33] H. Bock, D.J. Diestler, and M. Schoen, J. Phys.: Condens. Matter **13**, 4697 (2001).
[34] T. Flebbe, B. Dünweg, and K. Binder, J. Phys. II **6**, 665 (1996).
[35] N.B. Wilding, F. Schmid, and P. Nielaba, Phys. Rev. E **58**, 2201 (1998).
[36] R. J. Baxter, *Exactly Solved Models in Statistical Physics* (Academic, London, 1991), Chap. 1.9.
[37] H. Bock and M. Schoen, Phys. Rev. E **59**, 4122 (1999).
[38] M. Thommes and G.H. Findenegg, Langmuir **10**, 4270 (1994).
[39] M. Müller, J. Chem. Phys. **116**, 9930 (2002).
[40] F. Joabsson and P. Linse, J. Phys. Chem. B **106**, 3827 (2002).
[41] H. Bock and M. Schoen, J. Phys.: Condens. Matter **12**, 1569 (2000).
[42] D. Woywod and M. Schoen (unpublished).